Hindawi Publishing Corporation
Modelling and Simulation in Engineering
Volume 2012, Article ID 867820, 15 pages
doi:10.1155/2012/867820

Research Article

CFD Parametric Studies for Global Performance Improvement of Open Refrigerated Display Cabinets

Pedro Dinis Gaspar,[1] L. C. Carrilho Gonçalves,[1] and R. A. Pitarma[2]

[1] *Electromechanical Engineering Department, University of Beira Interior, Rua Fonte do Lameiro, Edificio 1 das Engenharias, 6201-001 Covilhã, Portugal*
[2] *Mechanical Engineering Department, High School of Technology and Management, Polytechnic Institute of Guarda, Avenida Dr. Francisco Sá Carneiro, No. 50, 6300-559 Guarda, Portugal*

Correspondence should be addressed to Pedro Dinis Gaspar, dinis@ubi.pt

Received 9 April 2012; Accepted 20 November 2012

Academic Editor: Antonio Munjiza

A detailed CFD modelling of an open refrigerated display cabinet has been formulated in a previous study. Some modifications are introduced in order to perform parametric studies dealing with low-cost geometrical and functional characteristics for improvement of the global performance and energy efficiency. The parametric studies are devoted to the analysis of the thermal response and behaviour inside the food conservation space influenced by (1) air flow rate through the evaporator heat exchanger; (2) air curtain behaviour; (3) hole dimensions and distribution of the back panel; (4) discharge and return grilles angles; and (5) flow deflectors inside the internal duct. The analysis of the numerical predictions from the parametric studies allows the development of an optimized model for the conception of an open refrigerated display cabinet with a more adequate configuration. The numerical predictions of the optimized model show lower product temperature and reduced electrical energy consumption, allowing the improvement of the food safety and the energy rationalization of the refrigeration equipment.

1. Introduction

Most of the refrigeration equipment installed in supermarkets are vertical refrigerated display cabinets opened to the surrounding air. A large part of the electrical supermarket energy consumption is due to these equipment [1]. This type of equipment uses an air curtain to reduce the external infiltration from the outside air at higher dry bulb temperature and specific humidity. The effectiveness of this aerothermodynamics barrier is affected by thermal and mass diffusive effects that increase the thermal entrainment, flow instabilities, and wall effects, among other characteristics, leading to less conservation quality of food products and larger energy consumption and costs. The ambient air infiltration load comprises around 67% to 77% of the cooling load of open refrigerated display cabinets (ORDC) [2]. The world demand for commercial refrigeration equipment is assumed to rise 5.2% annually through 2014, being the sales market headed by reach-in and walk-in coolers and freezers due to their widespread use in all of the major markets. Display cabinets will benefit from a growing middle class, which will spur gains in the food and beverage retail segment [3]. Also, the effects of the climatic change predictions [4, 5], characterized by an increase of the mean air temperature and the reduction of precipitation, the increasing sensitization for energy rationalization and sustainability, and the society requirements for food quality and safety, foster the need to carry out deeper studies and research on the behaviour of this type of food refrigeration equipment.

Due to the increasing energy demand, the research work in this field, both experimental and numerical, focus on the air curtain installed in the ORDC. Smale et al. [6] and Norton and Sun [7] presented a review of the application of Computational Fluid Dynamics (CFD) and other numerical modelling techniques to predict of air flow in refrigerated food applications including cool stores, transport equipment and retail display cabinets. Among these studies, several CFD studies were developed combining experimental techniques

to improve both the aerothermodynamics performance of the air curtain and the thermal energy efficiency of vertical ORDC. Several researchers carried out parametric studies based on two- (2D) and three-dimensional (3D) CFD models. Cortella et al. [8] evaluated the influence of air jet velocities in the thermal performance and determine the energy balance of the ORDC. The latter was obtained by the quantification of the air infiltration through the frontal opening. Navaz et al. [9] performed a CFD parametric study to determine the influence of the average velocity and temperature of the discharged air on the ambient air infiltration rate. They concluded that the infiltration rate is a very weak function of the discharge air grille (DAG) temperature and is mostly momentum driven. Axell and Fahlén [10] propose a method to evaluate the aerothermodynamics performance of the air curtain taking into account the storage temperature and the air curtain stability. A CFD parametric study was developed to evaluate the influence of the height/width ratio and inlet velocity of the air curtain on the performance. Navaz et al. [11] propose a CFD parametric study to calculate the amount of entrained air as a function of the Reynolds number based on the jet width and velocity, and inlet turbulence intensity, with the objective to determine the optimum operating conditions. These authors concluded that reducing turbulence intensity at the DAG reduces the entrainment for Reynolds numbers within a range from transitional to fully turbulent regime. Nevertheless, it cannot be decreased to a laminar regime since it will present negative effects in the food product temperature. The momentum reduction will increase the air temperature returned to the evaporator.

Foster et al. [12] provide 3D CFD modelling concentrated on two areas of the ORDC: the flow area on the rear duct downstream the evaporator and the area in the upper shelf of the food products conservation region. CFD modelling was used to investigate the effect of changing the size and position of the evaporator coil and inserting baffle plates into the duct, in the flow up the rear duct. Other CFD model was used to investigate the effect of changing the width and angle of the curtain in order to optimize the air curtain for the top shelf. The CFD model considering the modification of the air curtain width predicts the top shelf vortex minimization. They concluded that the optimum air curtain angle depends on the width and velocity of the curtain. Chen [13] developed CFD parametric studies to evaluate the thermal barrier performance of air curtains, adjusting the length/width ratio and its discharge angle; the height/depth ratio of the cavity; and the dimensions and position of shelves.

Chen and Yuan [14] developed an experimental study to evaluate the influence of several effects: ambient temperature and relative humidity; indoor air flow; DAG velocity; air flow accross the perforated back panel (PBP); and night covers application, on the performance of an ORDC. The results show that temperatures inside the food products conservation area and heat gains increase with ambient air temperature and relative humidity. The air flow parallel to the ORDC is not to significant for the thermal performance, but the increase of the DAG velocity increases the homogeneity of the air temperature in the food products conservation area and decreases the temperature difference between the returned and discharged air and thus lowering the heat gain. The holes density modification of the PBP can reduce the inside temperature, while night covers have efficacy for energy savings. Gray et al. [15] also conducted an experimental study to evaluate the effect of the perforation pattern of the back panel on the distribution of airflow. They concluded that a flow distribution of 70% through the curtain and 30% through the back panel perforation yields a performance that satisfies the standards. D'Agaro et al. [16] developed a steady and transient 2D and 3D modelling of the air flow in an ORDC to evaluate the importance of 3D effects on the performance. Parametric studies were carried out to evaluate the influence of the: longitudinal ambient air movement; ORDC length, and air curtain temperature. The predictions indicate that the extremity effects are particularly important in the case of cabinets of reduced length.

The above-mentioned works consider the CFD modelling for an ORDC, but all of them consider prescribing the discharge air grille (DAG) and return air grille (RAG) temperature and velocity as inflow and outflow boundary conditions, respectively, besides others experimental results used at the boundaries.

The work described in this study intends to combine the characteristics of the aforementioned works, where the parametric studies are developed in a different basis using the CFD model of an ORDC developed by Gaspar et al. [17]. This previous study performed a detailed CFD modelling of air flow and heat transfer in an ORDC. The physical-mathematical model considered the flow through the internal ducts, across fans and evaporator, and includes the thermal response of food products. The air flow and non-isothermal heat transfer process are modelled by a 2D (length mid-plane neglecting extremity effects) steady state model. The basic equations governing transport phenomena are continuity, momentum, and energy. The airflow modelling is coupled to products modelling, where within the latter region the convection term is neglected. The air is considered as an ideal gas. Considering that flow can be driven by buoyancy forces in specific zones of the domain, the Buossinesq approximation is applied. Turbulence is modelled by the RNG k-ε model. The influence of ambient air relative humidity is considered using a species transport model. The fluid is considered as a mixture of dry bulb air and water vapour. A surface-to-surface radiation model (based in surfaces view factors calculation) is used to take this heat gain component into account. The set of coupled non-linear partial differential equations, describing mass, momentum and energy conservation was simultaneously and interactively solved by the finite volume method on the CFD code FLUENT for the non-structured grid with 110 029 cells. PISO algorithm [18] was used for pressure-velocity coupling and the equations were discretized in the control volume form using MUSCL differencing scheme [19].

Experimental testing followed the procedure defined by EN-ISO Standard 23953 [20] for test room climate class no. 3, which considers air temperature, $T_{amb} = 25^{\circ}C$; air relative humidity, $\phi_{amb} = 60\%$; air velocity magnitude,

Table 1: Fans main technical characteristics.

Case study	Fan reference (EBM Papst)	Air flow rate Q [m^3 s^{-1}]	Rotation speed ω [rpm]	Power P [W]
BCS	4500N	0.0469	3000	15.0
OPTv1	4300H	0.0570	3400	11.0
OPTv2	4600N	0.0500	3100	18.0
OPTv3	4400F	0.0472	2900	5.5
OPTv4	4300N	0.0488	3150	4.5
OPTv5	4300	0.0472	2800	5.0

Table 2: Fan boundary condition: Fan pressure characteristic curves—OPTv case study.

Case study	Pressure characteristic curve
BCS	$\Delta p = -1.61v^4 - 2.67v^3 + 22.7v^2 - 51.1v + 79.2$
OPTv1	$\Delta p = -8.14v^4 + 39.99v^3 - 56.83v^2 - 11.53v + 94.72$
OPTv2	$\Delta p = -5.67v^4 + 0.86v^3 + 0.12v^2 - 0.04v + 98.80$
OPTv3	$\Delta p = -7.16v^4 + 24.52v^3 - 18.97v^2 - 23.40v + 54.57$
OPTv4	$\Delta p = -8.02v^4 + 31.49v^3 - 27.09v^2 - 37.11v + 80.37$
OPTv5	$\Delta p = -8.43v^4 + 30.75v^3 - 23.78v^2 - 36.55v + 70.48$

$v_{\text{amb}} = 0.2\,\text{m s}^{-1}$, with direction parallel to the frontal opening plane of the ORDC, that is, $\theta_{\text{amb}} = 0°$, and for M-package temperature class M1 ($1°\text{C} \le T_{\text{prod}} \le 5°\text{C}$). The experimental data was used to define boundary conditions and to validate the numerical predictions of air temperature, relative humidity and velocity. Numerical and experimental results comparison reveals the predictive capabilities of the computational model for the optimized conception and development of this type of equipment.

The analysis of numerical predictions of air flow and temperature performed in this previous work provides the assessment of geometrical and functional modifications concerning the conception, the project, and development of ORDC in order to improve its global performance behaviour. This CFD model, from now on named as Base Case Study (BCS) was adapted in order to accommodate the geometry modifications required by the parametric studies. Thus, the variables calculated along the BC specification process (pressure drop and equivalent global heat transfer coefficient at the evaporator, viscous and inertial resistance coefficients at the PBP, RAG, and DAG) were recalculated in accordance to the specific case study details.

2. Parametric Studies

The objective of the following case studies is to promote a better distribution of air temperature, relative humidity, and velocity inside the ORDC taking into account several geometrical and functional modifications. Moreover, the working conditions improvement allows increasing the ORDC global performance, by the increasing of the air curtain efficacy which is related with the infiltration heat gain reduction.

2.1. Influence of the Fans Velocity. The DAG velocity and the height/width ratio of the air curtain possess high influence in the air curtain performance [10, 13, 14, 21–24]. According to Hayes and Stoecker [25], the deflection modulus, D_m (1), describes the ability to provide proper sealing of an ORDC to the surroundings. This dimensionless number represents the ratio of air curtain momentum to the magnitude of the pressure difference produced by horizontal forces, caused by temperature difference in either side of the air curtain (stack effect). The stack effect is created by the difference in air densities on the two sides of the opening and results in a linear variation in pressure from the top to the bottom. In the analytical model to assist in the design of air curtains provided by [25], the minimum value of the D_m for proper air curtain sealing lies between 0.12 and 0.25 when the turbulence intensity is less than 1%, and with a height/width (H/b) ratio between 10 and 100:

$$D_m = \frac{(\rho b v^2)_{\text{discharge}}}{gH^2\,|\rho_{\text{cons}} - \rho_{\text{amb}}|}. \tag{1}$$

Considering the numerical predictions of [17] and rearranging (1), the DAG velocity should be comprised between $1.55\,\text{m s}^{-1}$ and $2.24\,\text{m s}^{-1}$. So, it can be increased to provide an aerothermodynamics barrier more efficient. Also, the thermal influence of ambient air can be defined by the thermal entrainment ratio without PBP airflow, X_0, as proposed by [26] and defined in (2). This equation result will be zero if the air curtain has no entrainment for $h_{\text{return}} = h_{\text{discharge}}$ (unreachable condition) and it will increase with RAG enthalpy, h_{return}. When the air at the RAG is all from the ambient air, $h_{\text{return}} = h_{\text{amb}}$, the thermal entrainment ratio will reach unity:

$$X_0 = \frac{h_{\text{return}} - h_{\text{discharge}}}{h_{\text{amb}} - h_{\text{discharge}}}. \tag{2}$$

Yu et al. [26] deducted the TEF formula with PBP airflow (3) based on TEF without PBP airflow:

$$\text{TEF} = (1 - \beta)X_0 + \beta X_0 X_{\text{PBP}}, \tag{3}$$

where β is the PBP airflow ratio given by

$$\beta = \frac{\dot{m}_{\text{PBP}}}{\dot{m}_{\text{PBP}} + \dot{m}_{\text{DAG}}}. \tag{4}$$

Table 3: Parameters specified at the evaporator, DAG, RAG, and PBP boundary conditions—OPTv case study.

Zone	Variable	Case study				
		OPTv1	OPTv2	OPTv3	OPTv4	OPTv5
Evaporator	Δp [Pa]	11.93	9.35	8.40	8.93	8.40
	U_{eq} [W m^{-2} K^{-1}]	1104.12	968.53	914.25	945.29	914.25
PBP	$C_2 \times 10^9$ [m^{-1}]	2.47	2.49	2.50	2.49	2.50
RAG	$C_2 \times 10^3$ [m^{-1}]	3.50	4.55	5.10	4.77	5.10
DAG	C_2 [m^{-1}]	11.80	15.33	17.21	16.10	17.21

Table 4: DAG velocity prediction values for the different cases—OPTv case study.

Variable	Case study					
	BCS	OPTv1	OPTv2	OPTv3	OPTv4	OPTv5
$v_{discharge}$ [m s^{-1}]	1.51	2.03	2.46	1.55	1.74	1.60

and X_{PBP} is the TEF for PBP airflow:

$$X_{PBP} = \frac{T_{PBP} - T_{DAG}}{T_{amb} - T_{DAG}}. \quad (5)$$

The overall values of the thermal entrainment ratio obtained by experimental tests [2] and numerical predictions analysis [17] were in the range TEF = 0.25 to 0.36, that are adequate with those values found by [13, 27] for the obtained Re (=5933) and Ri (=0.029). Thus, this parametric study considers the CFD simulation for different fan characteristic curves (OPTv1 to OPTv5 cases). The fans selected for the OPTv cases study are from the same manufacturer (EBM), with the same dimension but with higher airflow rate, in order to analyse the influence of fans velocity in the ORDC performance. Additionally, these fans have lower electrical power consumption. Their technical characteristics are shown in Table 1.

The boundary condition (BC) of discontinuous pressure rise across the fan (infinitely thin face) is specified as a function of the velocity through it. The pressure characteristic curves which govern the relationship between head pressure and flow rate (velocity) across the fan element are represented by a 4th order polynomial relationship (Table 2) specified as BC. These polynomials were obtained using the least minimum squares method to find the approximate functions that characterize the pressure characteristic curves of fans.

Due to fans velocity modification, several BC are reformulated, namely, the heat and mass transfer and pressure drop modelling across the evaporator, the air pressure drop across the PBP and the DAG and RAG are modelled as porous medium. The BC values are shown in Table 3. The values of the DAG velocity predictions for the different cases ares shown in Table 4.

Following the procedure exposed in [17], a region that enclosures virtually the air curtain boundaries is considered. These virtual boundaries are subdivided in 5 control volumes (VC) as shown in Figure 1. The mass flow (6) and the heat

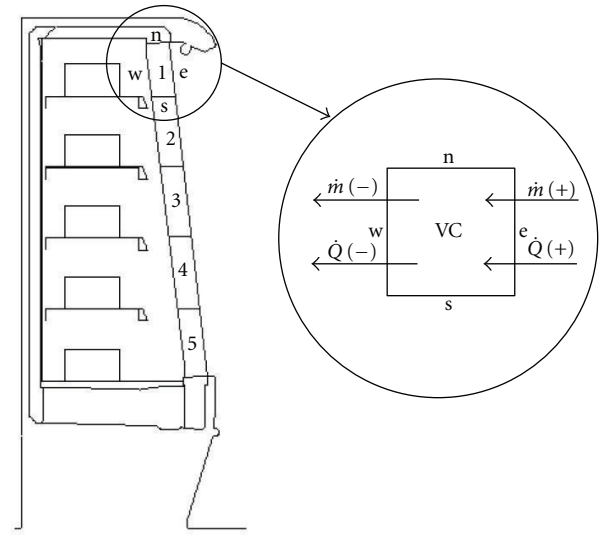

Figure 1: Subdivision of the air curtain region by control volumes and sign convention of the variables.

transfer (7) rates across the air curtain per unit length were determined for each VC:

$$\dot{m} = \rho v A \left[\text{kg s}^{-1}\right], \quad (6)$$

$$\dot{Q} = \dot{m} C_p \Delta T_1 \text{ [W]}. \quad (7)$$

The values and directions of the heat transfer across the air curtain by unit length are shown in Figure 2. These predictions indicate thermal energy gains of the air curtain from the external ambient and conservation region for all case studies. These thermal gains are related to the ambient air infiltration, thermal radiation, illumination, and heat conduction through the wall of the ORDC.

In OPTv1, OPTv2, and OPTv4 are predicted larger DAG velocities than in the BCS, as well as larger mass flow rates and heat transfer rates through the inner and outer borders of the air curtain. The mass flow rate across the inner border promotes the mixture between the refrigerated

Table 5: Thermal and temperature ratios relatively to BSC—fans velocity parametric study.

	Case study				
	OPTv1	OPTv2	OPTv3	OPTv4	OPTv5
TEF	+2.8%	+3.5%	**+0.6%**	−0.4%	0.9%
$\{(\dot{Q}_{\mathrm{OPTv}} - \dot{Q}_{\mathrm{BCS}})/\dot{Q}_{\mathrm{BCS}}\}_{\mathrm{total,sen}}$	+12.0%	+33.2%	**−16.3%**	−8.0%	−13.5%
$\{(\dot{Q}_{\mathrm{OPTv}} - \dot{Q}_{\mathrm{BCS}})/\dot{Q}_{\mathrm{BCS}}\}_{\mathrm{total,lat}}$	+10.4%	+40.3%	**−18.0%**	−9.1%	−14.1%
$\{(T_{\mathrm{OPTv}} - T_{\mathrm{BCS}})/T_{\mathrm{BCS}}\}_{\mathrm{discharge}}$	−0.7%	−6.1%	**−20.3%**	+2.1%	−9.2%
$\{(T_{\mathrm{OPTv}} - T_{\mathrm{BCS}})/T_{\mathrm{BCS}}\}_{\mathrm{return}}$	+2.1%	−1.3%	**−4.7%**	+0.8%	−1.8%
$\{(T_{\mathrm{OPTv}} - T_{\mathrm{BCS}})/T_{\mathrm{BCS}}\}_{\mathrm{cons}}$	+12.1%	−40.5%	**−43.4%**	−0.4%	−26.3%
$\{(T_{\mathrm{OPTv}} - T_{\mathrm{BCS}})/T_{\mathrm{BCS}}\}_{\mathrm{prod}}$	−5.0%	−4.5%	**−7.6%**	−5.2%	−7.6%

Table 6: Parameters specified at PBP boundary conditions—OPTp case study.

Case	Parameter designation	Variable	Unit	PBP height, z [%]		
				[0 40]	[40 60]	[60 100]
BCS	Diameter	D_{hole}	[mm]		4.25	
	Porosity	ε	[%]		2.6	
	Viscous resist. coef.	k^{-1}	[m^{-2}]		2.56×10^7	
	Inertial resist. coef.	C_2	[m^{-1}]		2.49×10^9	
OPTp1	Diameter	D_{hole}	[mm]		8.50	
	Porosity	ε	[%]		10.45	
	Viscous resist. coef.	k^{-1}	[m^{-2}]		1.59×10^6	
	Inertial resist. coef.	C_2	[m^{-1}]		8.42×10^6	
OPTp2	Diameter	D_{hole}	[mm]	8.50		4.25
	Porosity	ε	[%]	10.84		2.55
	Viscous resist. coef.	k^{-1}	[m^{-2}]	1.53×10^6		2.61×10^7
	Inertial resist. coef.	C_2	[m^{-1}]	7.23×10^6		2.74×10^9
OPTp3	Diameter	D_{hole}	[mm]	4.25	8.50	
	Porosity	ε	[%]	2.65	10.14	
	Viscous resist. coef.	k^{-1}	[m^{-2}]	2.51×10^7	1.64×10^6	
	Inertial resist. coef.	C_2	[m^{-1}]	2.35×10^9	9.54×10^6	

air discharged by the air curtain and the food products conservation air. When followed by an increase of the mass flow rate that crosses the outer border, there is an increase of the thermal entrainment reducing the air curtain efficiency. It was found that the applicability of the deflection modulus is restricted for air curtains installed in ORDC, as it does not considers the plug flow from the PBP. The values for an efficient aerothermodynamics barrier should be close to the minimum value of the range obtained by the D_m calculation.

The OPTv2 case is the only one predicting a DAG velocity greater than the maximum limit obtained through the deflection modulus (1), $v_{\mathrm{discharge}} = 2.24\,\mathrm{m\,s^{-1}}$. Globally, in this case are predicted the higher mass flow and heat transfer, both in and out the faces of the outer border of the air curtain, revealing the applicability of this nondimensional parameter. This larger fan velocity also provides a larger mass flow rate through the PBP. For the remainder case studies, the predicted DAG velocity are within the range obtained by D_m calculus. However, only OPTv3 and OPTv5 provide a proper aerothermodynamics barrier. The DAG velocity value in these models is near the minimum limit ($v_{\mathrm{discharge}} = 1.55\,\mathrm{ms^{-1}}$) obtained through the deflection modulus, Dm, calculation (1). These findings are in agreement with the air temperature predictions shown in Figure 3. Table 5 shows the variation of thermal characteristics for the different case studies in relation to BCS. It includes the TEF as well as the total thermal load subdivided in the sensible and latent components (determined by (8) and (9), resp.), the DAG and RAG temperatures, the air temperature in the food products area, and the internal food products temperature:

$$\dot{Q}_{\mathrm{total,sen}} = (\rho v A)_{\mathrm{discharge}} \left(h_{\mathrm{return}} - h_{\mathrm{discharge}}\right), \quad (8)$$

$$\dot{Q}_{\mathrm{total,lat}} = (\rho v A)_{\mathrm{discharge}} h_{fg} \left(\omega_{\mathrm{return}} - \omega_{\mathrm{discharge}}\right). \quad (9)$$

The OPTv3, OPTv4, and OPTv5 show small differences in the air infiltration thermal load relatively to the BSC due to larger fans flow rate. TEF comparison among the case studies shows small varitions relatively to BCS. The comparison of the numerical predictions of the different case studies indicates that OPTv3 fan can improve the global performance of the ORDC.

Table 7: Thermal and temperature ratios relatively to BSC—density and distribution perforation parametric study.

	Case study		
	OPTp1	OPTp2	OPTp3
TEF	**−20.7%**	−11.8%	−10.5%
$\left\{(\dot{Q}_{\mathrm{OPTp}} - \dot{Q}_{\mathrm{BCS}})/\dot{Q}_{\mathrm{BCS}}\right\}_{\mathrm{total,sen}}$	**−30.8%**	−25.5%	−25.5%
$\left\{(\dot{Q}_{\mathrm{OPTp}} - \dot{Q}_{\mathrm{BCS}})/\dot{Q}_{\mathrm{BCS}}\right\}_{\mathrm{total,lat}}$	**−33.9%**	−27.6%	−27.4%
$\left\{(T_{\mathrm{OPTp}} - T_{\mathrm{BCS}})/T_{\mathrm{BCS}}\right\}_{\mathrm{discharge}}$	**−8.4%**	−7.2%	−7.7%
$\left\{(T_{\mathrm{OPTp}} - T_{\mathrm{BCS}})/T_{\mathrm{BCS}}\right\}_{\mathrm{return}}$	**−9.1%**	−6.5%	−6.4%
$\left\{(T_{\mathrm{OPTp}} - T_{\mathrm{BCS}})/T_{\mathrm{BCS}}\right\}_{\mathrm{cons}}$	**−3.9%**	+10.0%	+10.5%

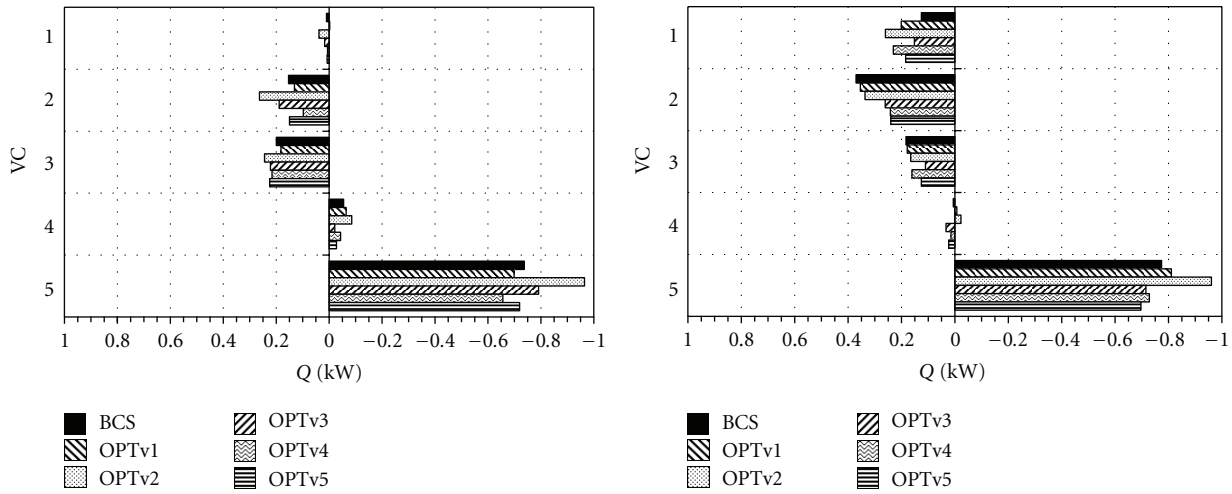

(a) West faces, w (inner border)

(b) East faces, e (outer border)

Figure 2: Enthalpic flow rate predictions across West (inner border) and East (outer border) of the air curtain control volumes, per unit length—OPTv cases study.

Table 8: DAG and RAG angles—grille angles parametric study.

Case study	Angles	
	RAG, γ_{return} [°]	DAG, $\gamma_{\mathrm{discharge}}$ [°]
BCS	−5.0	5.0
OPTγ1	−5.0	0.0
OPTγ2	0.0	0.0
OPTγ3	−10.0	5.0
OPTγ4	−10.0	0.0
OPTγ5	0.0	5.0
OPTγ6	−10.0	2.5
OPTγ7	−10.0	−2.5

2.2. Diameter and Density Perforation of the Back Panel. As presented by [13–15] and verified by the experimental and numerical results in [17], the largest air temperature is found in the well tray. This parametric study predicts the effects of holes dimension of PBP, uniformly and nonuniformly distributed, on the distribution of the air temperature field. The BSC has a uniform perforation with $D_{\mathrm{hole}} = 4.25$ mm. The case studies have a double hole diameter, $D_{\mathrm{hole}} = 8.5$ mm uniformly distributed (OPTp1), and a nonuniform perforation pattern, respectively. For the latter case study, the first 2/5 of PBP height has a $D_{\mathrm{hole}} = 8.5$ mm while in the remainder height it has the original hole diameter (OPTp2). The last case study (OPTp3) considers the reverse perforation distribution.

Likewise the previous parametric study, these modifications require the reformulation of the values specified at the BC. These parameters are related to the porous medium formulation used to simulate the PBP. The values of porosity, ε, viscous, k^{-1}, and inertial, C_2, resistance coefficients calculated as exposed in [17] are recalculated and shown in Table 6.

The flow rate by the PBP increases and the air flow rate through the DAG reduces with the increase of the holes diameter. The values and directions of the heat transfer rates across the air curtain by unit length are shown in Figure 4. The comparative analysis of the numerical predictions of the case studies indicates that the vortex formation in the top shelf is suppressed by the reduction of DAG velocity. These modifications increase the mass flow and heat transfer rates through the outer border of the air curtain and decrease them in the inner border, being the differences not so pronounced. The numerical predictions indicate that the reduction of DAG velocity reduces the thermal entrainment at top height

Table 9: Thermal and temperature ratios relatively to BSC—grille angles parametric study.

	Case study						
	OPTγ1	OPTγ2	OPTγ3	OPTγ4	OPTγ5	OPTγ6	OPTγ7
TEF	+10.2%	+9.7%	+8.5%	+10.4%	+8.0%	+8.6%	+12.8%
$\left\{\left(\dot{Q}_{\mathrm{OPT}\gamma} - \dot{Q}_{\mathrm{BCS}}\right)/\dot{Q}_{\mathrm{BCS}}\right\}_{\mathrm{total,sen}}$	+6.5%	+6.2%	+4.3%	+7.0%	+4.0%	+3.4%	+11.2%
$\left\{\left(\dot{Q}_{\mathrm{OPT}\gamma} - \dot{Q}_{\mathrm{BCS}}\right)/\dot{Q}_{\mathrm{BCS}}\right\}_{\mathrm{total,lat}}$	+15.5%	+14.6%	+11.6%	+16.0%	+11.2%	+11.3%	+21.2%

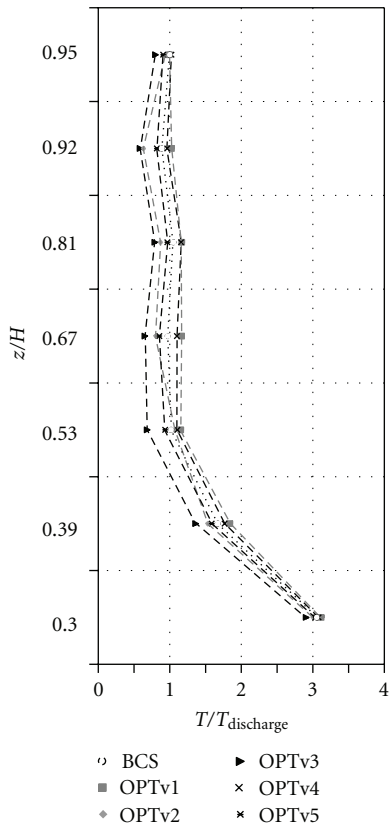

Figure 3: Comparative profiles of nondimensional air temperature, $T/T_{\mathrm{discharge}}(y/W = 0.44, z/H)$, in the conservation zone—OPTv cases study.

of the air curtain (near DAG) but increases it at the bottom height (near RAG) due to air curtain momentum reduction. This situation is verified by the analysis of the mass flow rate at the lowest control volume (VC 5) and by the analysis of the air temperature and velocity profiles shown in Figures 5 and 6. These modifications accomplish a reduction of the air temperatures near the PBP and at the evaporator return. The comparison of the thermal characteristics of the different case studies in relation to BCS is shown in Table 7.

The increase of mass flow rate through the PBP allows the reduction of the DAG and RAG temperatures and consequently the TEF reduction. A reduction of the air temperature in the food products conservation area is predicted only in the OPTp1 case study. Based on these numerical results, it is proper to double the perforation diameter with uniform distribution to reduce the thermal load and air temperature.

2.3. Discharge and Return Air Grille Angles. Several authors related the stability and efficiency of the air curtain to the air jet discharge angle [19, 27]. This parametric study evaluates the angle, γ, of DAG and RAG on the global performance of the ORDC. BCS has a $\gamma_{\mathrm{discharge}} = 5^{\circ}$ (positive angle is measured to the ambient side) and $\gamma_{\mathrm{return}} = -5^{\circ}$ (negative angle is measured to the internal side). The following constraints were assumed based in experimental tests: (1) the air is discharged totally to the ambient air for $\gamma_{\mathrm{discharge}} > 6^{\circ}$, increasing both the leakage of cold air to the ambient and the air temperature at the RAG. These situations lead to a refrigeration capacity loss; and (2) the maximum DAG angle that does not disrupts the air curtain is $\gamma_{\mathrm{discharge}} = -2.5^{\circ}$ (limited by shelves position). The different case studies modelled are shown in in Table 8.

The CFD models made use of the mathematical and numerical formulations exposed by [17] but required geometry modifications and new mesh generation. The automatic mesh generator included in the software Gambit was used. Although all geometrical faces have the same number of control volumes, the computational models have slight variations on the total number of control volumes.

The values and directions of the heat transfer across the air curtain by unit length are shown in Figure 7. The numerical predictions analysis indicates that the reduction of the DAG angle (OPTγ1, OPTγ2, OPTγ4, OPTγ6, and OPTγ7) increase the mass flow rate and the heat transfer across the outer border of the air curtain in the top height (VC 1). The case studies with the same DAG angle as BCS (OPTγ3 and OPTγ5) show larger mass flow rate in the outer border (face east) in the control volume (VC 2) below. The DAG angle influence is reduced at the bottom height, presenting all cases similar predictions. The variation of TEF and total thermal load (sensible and latent components) of the different case studies in relation to BCS is shown in Table 9.

When the DAG angle is $\gamma_{\mathrm{discharge}} = 0^{\circ}$ or smaller (OPTγ1, OPTγ2, OPTγ4, and OPTγ7 cases), the air infiltration thermal load increases as well as the total thermal load due to disruption of air curtain by shelves obstruction. From the analysis of the numerical predictions, there is no influence of the RAG angle on the ORDC performance. For DAG velocity, $v_{\mathrm{discharge}}$, lower than $2\,\mathrm{m\,s^{-1}}$, the influence of the DAG and RAG angles in the global performance is negligible comparing with the previous parametric studies results. From the comparison between the case studies, OPTγ6 is the

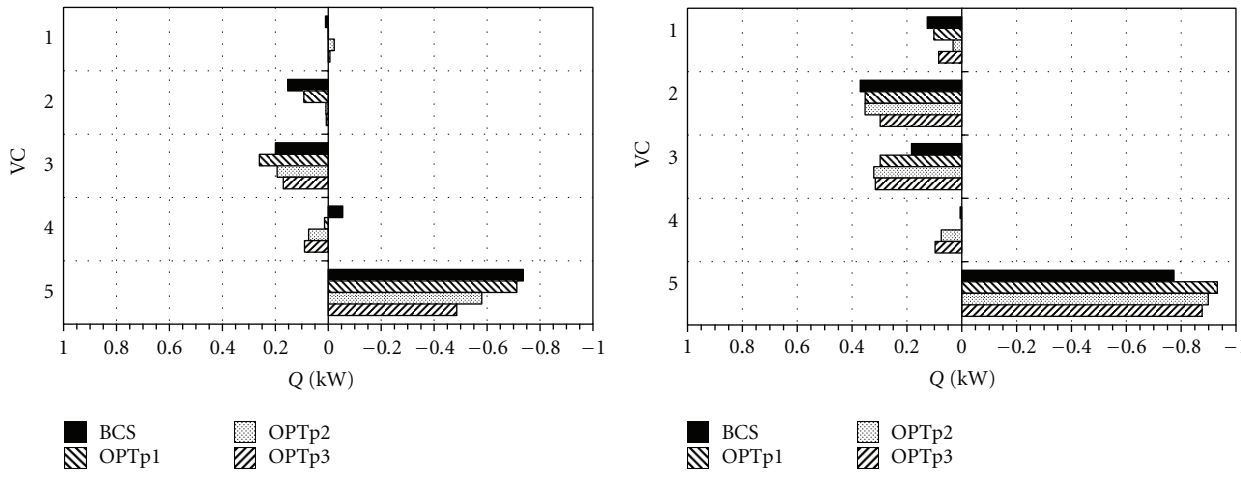

(a) West faces, w (inner border)

(b) East faces, e (outer border)

Figure 4: Enthalpic flow rate predictions across West (inner border) and East (outer border) of the air curtain control volumes, per unit length—OPTp cases study.

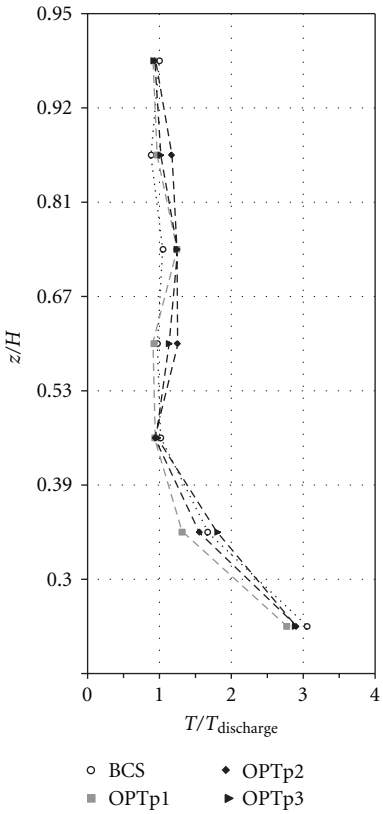

Figure 5: Comparative profiles of nondimensional air temperature, $T/T_{\text{discharge}}(y/W = 0.44, z/H)$, in the conservation zone—OPTp cases study.

case study that provides a more stable air curtain, presenting a mass flow rate at the outer border of the air curtain directed to the interior with a similar trend as the BCS. This condition allows a reduction of the mass flow rate which escapes to the ambient. The inner border is crossed by a higher mass flow rate, which allows a better mixture between the air discharged by the DAG and the air in the food products area. However, all case studies present larger values of TEF than the BCS.

2.4. Internal Duct Deflectors (Guides and Convergents). Through the analysis of the numerical predictions [17] and as exposed by [12], the modification of the flow direction inside the internal duct using flow guides and/or convergents should allow to suppress the recirculation predicted in this area, improving the ORDC performance. This parametric study considers the modification of the internal duct flow using deflectors upstream the DAG, downstream the RAG and at the directions change between the rear and upper duct.

As in the previous parametric study, the CFD model (OPTd) made use of the mathematical and numerical formulations exposed in [17], but it required geometry alteration and new mesh generation. The geometrical modifications proposed in the internal duct are shown in Figure 8.

The values and directions of the heat transfer across the air curtain by unit length are shown in Figure 9.

The analysis of the numerical predictions indicates a small increase of the heat transfer through the outer border of the air curtain due to an increase of 2.4% of the DAG velocity. The heat transfer through the outer face of the VC located at the top height (VC 1) is directed to the exterior. Nevertheless, this condition increases the vortex formation downward this location (VC 2 and VC 3), increasing the total heat transfer through the outer border of the air curtain that is directed to the food products area. This situation is verified by the air temperature and velocity profiles of the air curtain shown in Figure 10. These modifications conduct to an increase of TEF (7.1%) and consequently of the air infiltration load (1.0%) and total thermal load (9.0%). As the results of the previous parametric study, the influence of

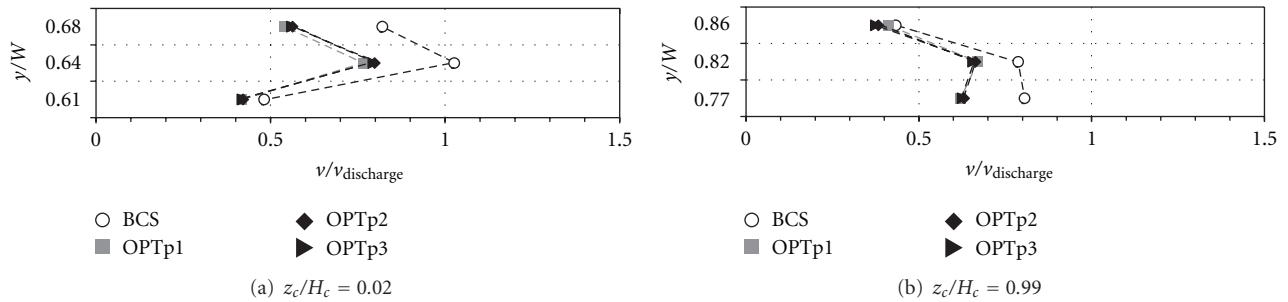

(a) $z_c/H_c = 0.02$ (b) $z_c/H_c = 0.99$

FIGURE 6: Comparative profiles of nondimensional air velocity, $v/v_{\text{discharge}}(y/W, z_c/H_c)$, in the air curtain—OPTp cases study.

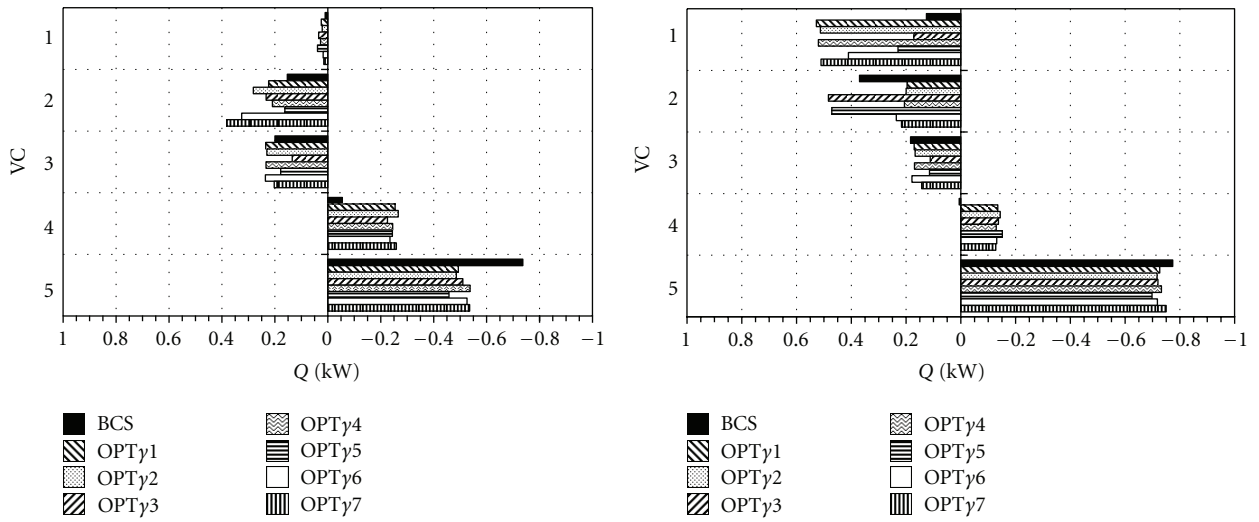

(a) West faces, w (inner border) (b) East faces, e (outer border)

FIGURE 7: Enthalpic flow rate predictions across West (inner border) and East (outer border) of the air curtain control volumes, per unit length—OPTγ cases study.

the flow direction modification inside the internal duct in the ORDC global performance is insignificant.

3. Global Optimization Performance Model

The analysis of the numerical predictions obtained with the previous parametric studies lead to the CFD modelling of an optimized ORDC. This CFD model, OPTg, considers the OPTv3 fan and the OPTp1 model with double holes diameter distributed uniformly along PBP. The DAG and RAG angles modification and the inclusion of flow guides and deflectors in the internal duct are not considered due to production costs and reduced influence on the ORDC performance as analysed in the specific case studies.

3.1. Velocity Field Predictions. The numerical predictions of the air velocity field for the computational domain and focusing the air curtain are shown in Figure 11. Comparing with the velocity profiles exposed in [17], larger velocity values in the food product area and lower values in the air curtain are predicted due to the larger mass flow rate through the PBP. The comparative profiles of the nondimensional air velocity at the air curtain are shown in Figure 12.

3.2. Temperature Field Predictions. The temperature distribution in the refrigerated display space is shown in Figure 13. The comparative profiles of nondimensional temperatures for the air in the air curtain, conservation zone, and internal food product are shown in Figures 14, 15, and 16, respectively. The numerical results show an average reduction of 1.8°C of the air temperature and its larger uniformity. Lower temperature values are predicted near the PBP. The internal temperature of products is not uniform but it has a lower average value (reduction of 1.2°C), being the products located in the shelves front more affected by the thermal entrainment and thermal radiation. Comparing with BCS, these temperature reductions improve the food safety.

3.3. Thermal Power across the Air Curtain. The values and directions of the heat transfer across the air curtain per unit length are shown in Figure 17. The analysis of the numerical

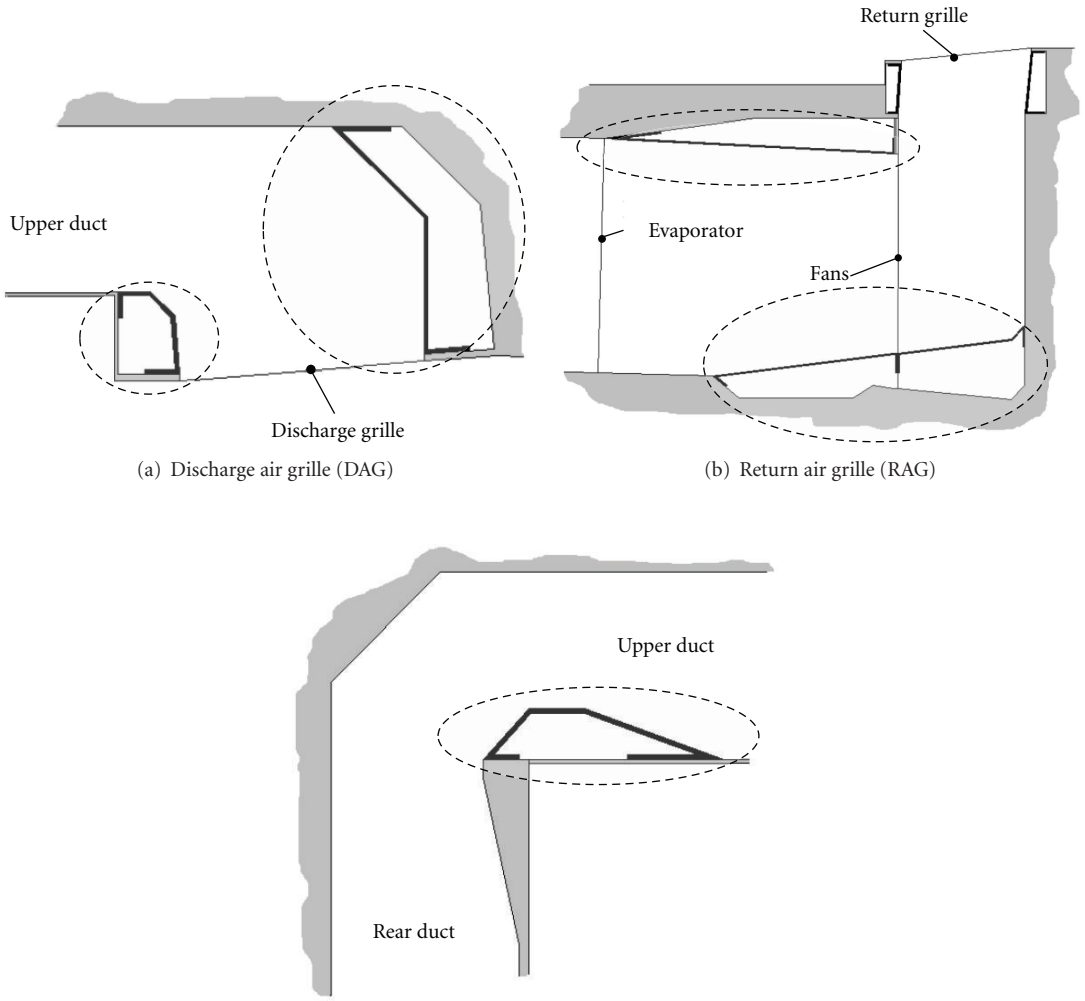

(a) Discharge air grille (DAG)

(b) Return air grille (RAG)

(c) Upper internal duct

Figure 8: Internal duct modifications.

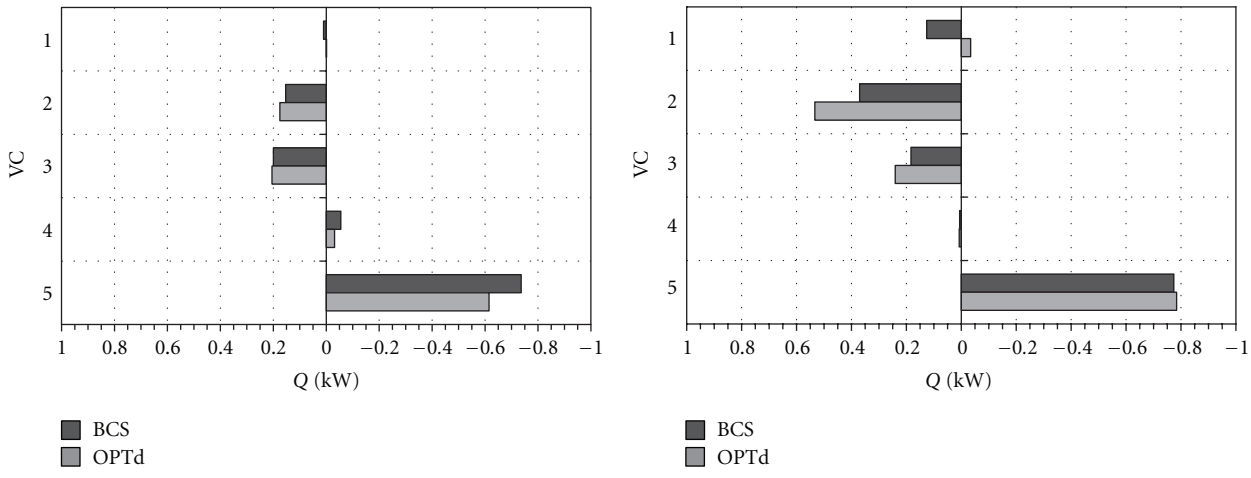

(a) West faces, w (inner border)

(b) East faces, e (outer border)

Figure 9: Enthalpic flow rate predictions across West (inner border) and East (outer border) of the air curtain control volumes, per unit length—OPTd case study.

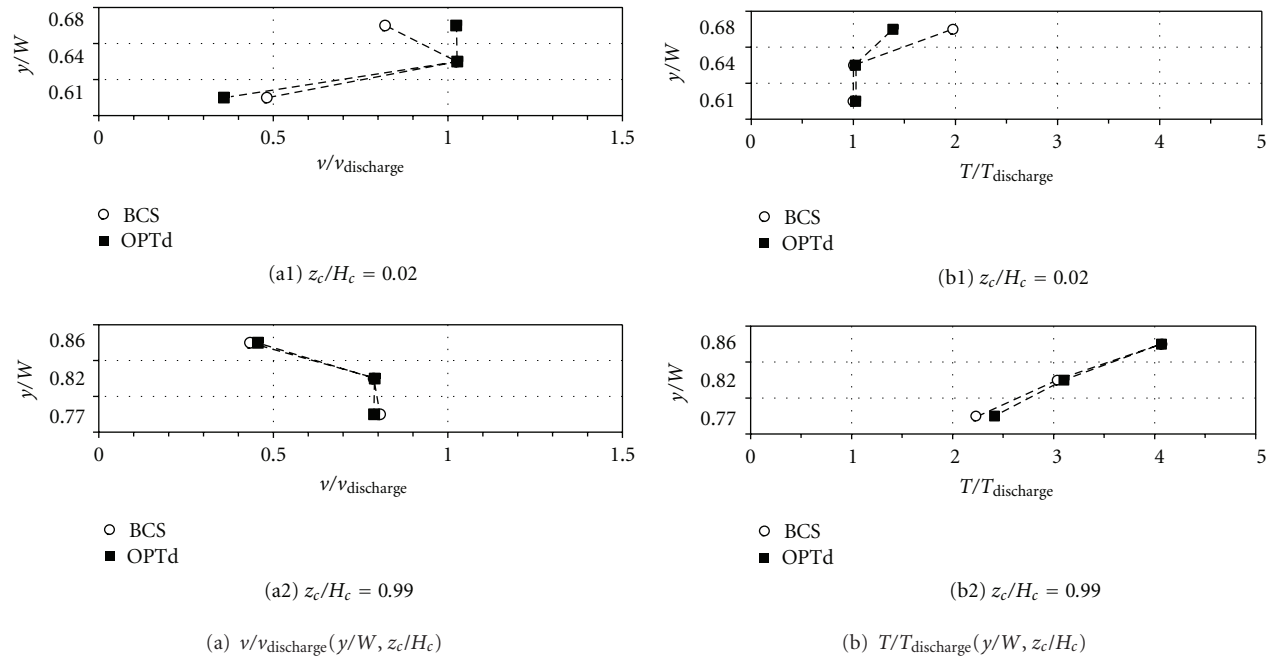

FIGURE 10: Comparative profiles of nondimensional air velocity, $v/v_{\text{discharge}}(y/W, z_c/H_c)$, and nondimensional air temperature, $T/T_{\text{discharge}}(y/W, z_c/H_c)$, in the air curtain—OPTd case study.

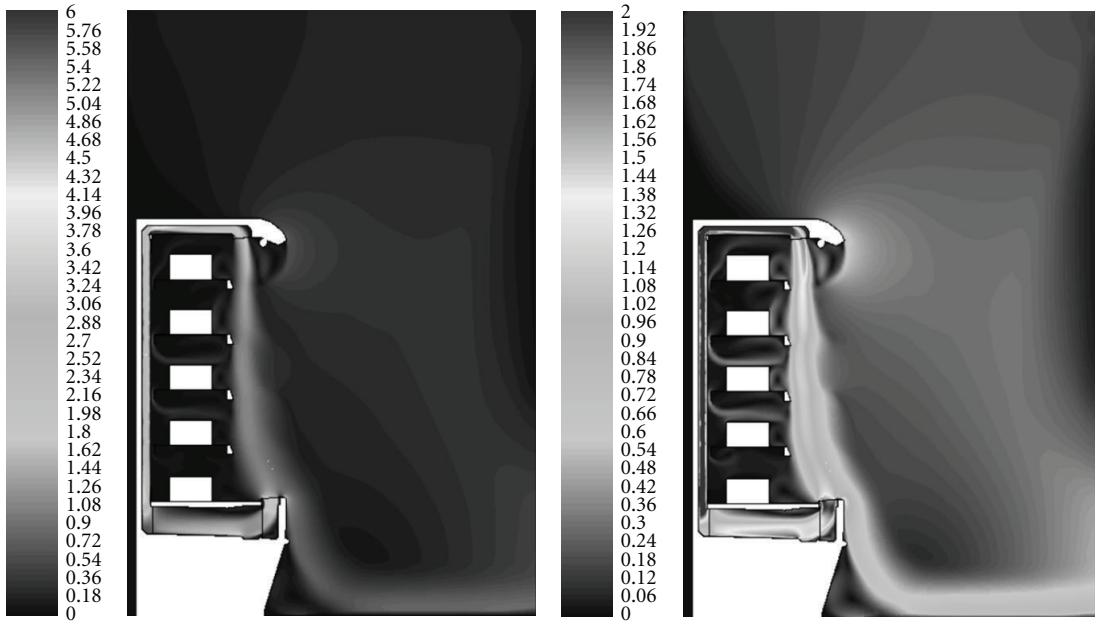

FIGURE 11: Velocity field numerical predictions, v [m s^{-1}]—OPTg case study.

predictions indicates a significant reduction of the thermal entrainment factor (43.5%) and an improvement of the air curtain efficacy. The reduction of the heat transfer through the outer border of the air curtain reduces the air infiltration load in 27.1% (414 W per unit length). Considering the total thermal load, it is predicted a reduction of 46.5% (900 W per unit length).

4. Conclusions

A CFD modelling of an open refrigerated display cabinet has been used to perform several parametric studies. It considers low-cost geometrical and functional modifications in order to forseen the global performance optimization and energy efficiency improvement. The parametric studies are devoted

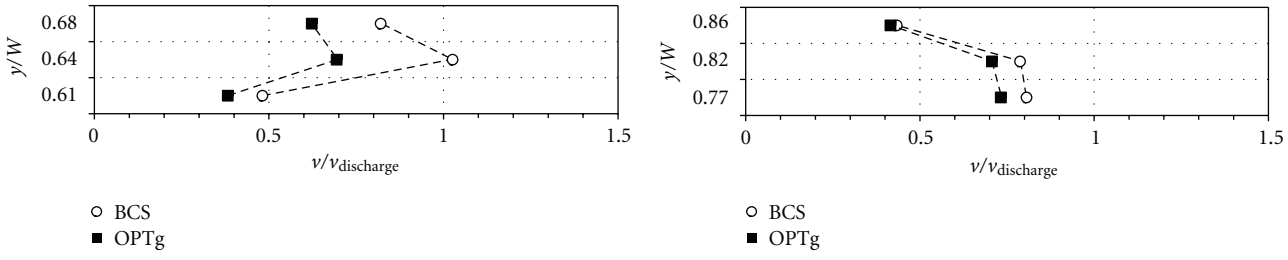

(a) $z_c/H_c = 0.02$ (b) $z_c/H_c = 0.99$

Figure 12: Comparative profiles of nondimensional air velocity, $v/v_{\text{discharge}}(y/W, z_c/H_c)$, in the air curtain—OPTg case study.

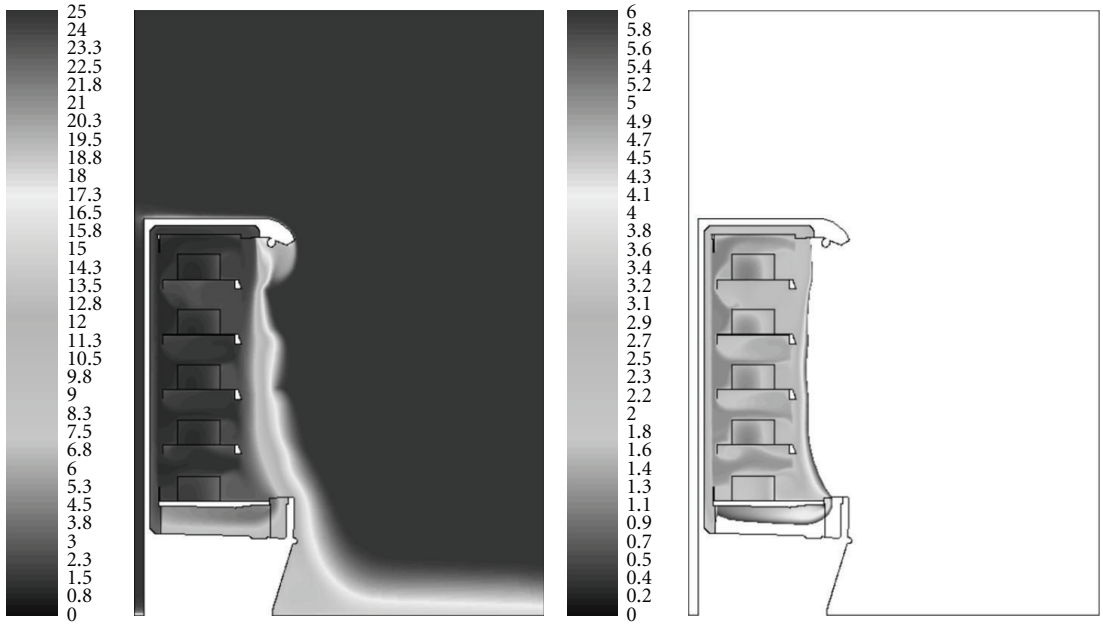

(a) Computational domain (b) Air curtain (reduced scale)

Figure 13: Temperature field numerical predictions, T [°C]—OPTg case study.

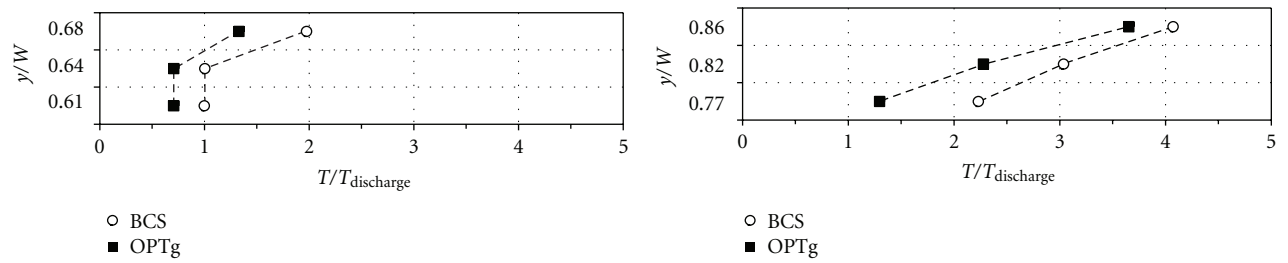

(a) $z_c/H_c = 0.02$ (b) $z_c/H_c = 0.99$

Figure 14: Comparative profiles of nondimensional air temperature, $T/T_{\text{discharge}}(y/W, z_c/H_c)$, in the air curtain—OPTg case study.

to the analysis of the thermal behaviour influenced by fans velocity, holes density and distribution on the PBP; DAG and RAG angles; and flow deflectors inside the internal duct.

The most promising numerical predictions of each parametric study were included in the CFD modelling of a modified display cabinet to predict and analyse its global performance optimization. The numerical results considering the proposed modifications predict a thermal entrainment factor reduction in 43.5% and an improvement of the air curtain efficacy. This condition leads to a reduction of 46.5% (900 W per unit length) of the total thermal load. Consequently, it is predicted a reduction of 1.8°C of the air temperature, which corresponds to a 1.2°C reduction of the food products internal temperature. Moreover, a more homogenous air temperature field and more uniform air velocity field are predicted. These results allow improving the

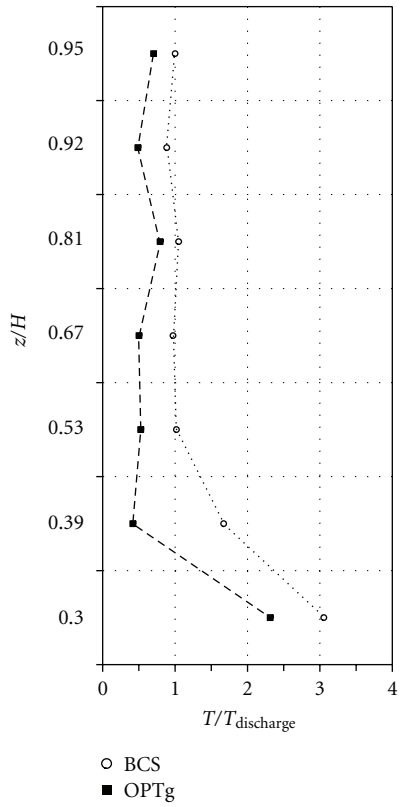

Figure 15: Comparative profiles of nondimensional air temperature, $T/T_{\text{discharge}}(y/W = 0.44, z/H)$, in the food products conservation area—OPTg case study.

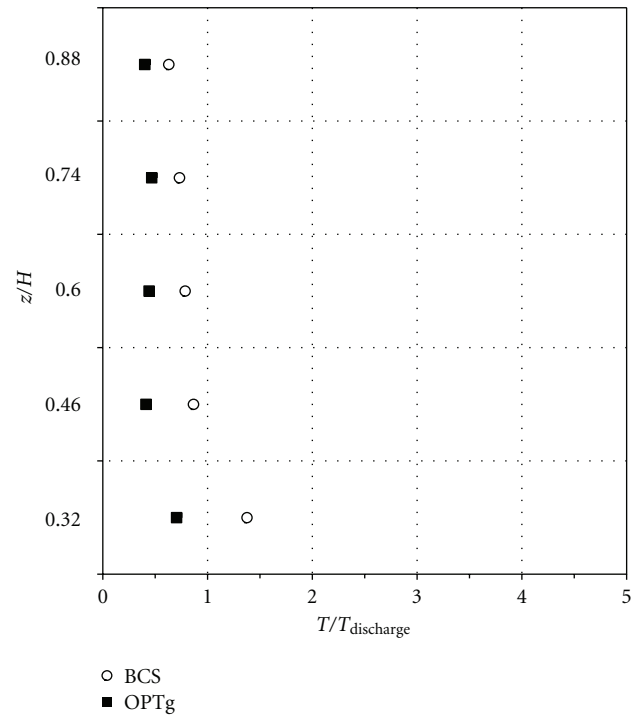

Figure 16: Comparative profiles of nondimensional internal food product temperature, $T/T_{\text{discharge}}(y/W = 0.33, z/H)$—OPTg case study.

food safety and increasing the conservation time period in cold. Additionally, the CFD model developed allows testing other relevant factors that may affect the global performance of the display cabinet, such as evaporator dimensions and its heat transfer rate, grilles grid, shelves width, among others.

The results of the numerical predictions using CFD as a design tool reveal the capabilities of this technique applied in an initial project phase, allowing testing several configurations with reduced cost and time. These numerical results can be used as design guides in order to obtain an improved final product in terms of energy consumption and food quality and safety facing the increasing exigencies from both sector regulation entities and consumers.

Nomenclature

A: Area (m^2)
b: Air curtain width, (m)
C_2: Inertial resistance coefficient, (m^{-1})
C_p: Specific heat, ($J\,g^{-1}\,K^{-1}$)
D: Diameter, (m)
g: Gravitational acceleration, ($m\,s^{-2}$)
h: Enthalpy, (Jkg^{-1})
H: Height, (m)
h_{fg}: Enthalpy of vaporization, ($J\,kg^{-1}$)
k^{-1}: Viscous resistance coefficient, (m^{-2})
L: Length, (m)
$\dot{m}$: Mass flow rate, ($kg\,s^{-1}$)
P: Electrical power, (W)
p: Pressure, (Pa)
Q: Volumetric flow rate, (m^3s^{-1})
$\dot{Q}$: Heat transfer rate, (W)
Re: Reynolds Number, $\text{Re} = ((\rho v D_h)/\mu)_{\text{discharge}}$
Ri: Richardson Number, $\text{Ri} = ((\rho_{\text{amb}} - \rho_{\text{discharge}})g b_{\text{discharge}})/(\rho_{\text{amb}} v^2_{\text{discharge}})$
T: Temperature, (°C)
U: Global heat transfer coefficient, ($W\,m^{-2}\,K^{-1}$)
v: Average velocity, ($m\,s^{-1}$)
x, y, z: Spatial coordinates, (m).

Superscripts and Subscripts

amb: Ambient
c: Air curtain
cons: Conservation
discharge: Air curtain discharge grille
e, w, n, s: Control volume faces identification (East, West, North, South)
eq: Equivalent
h: Hydraulic
hole: Back panel hole perforation

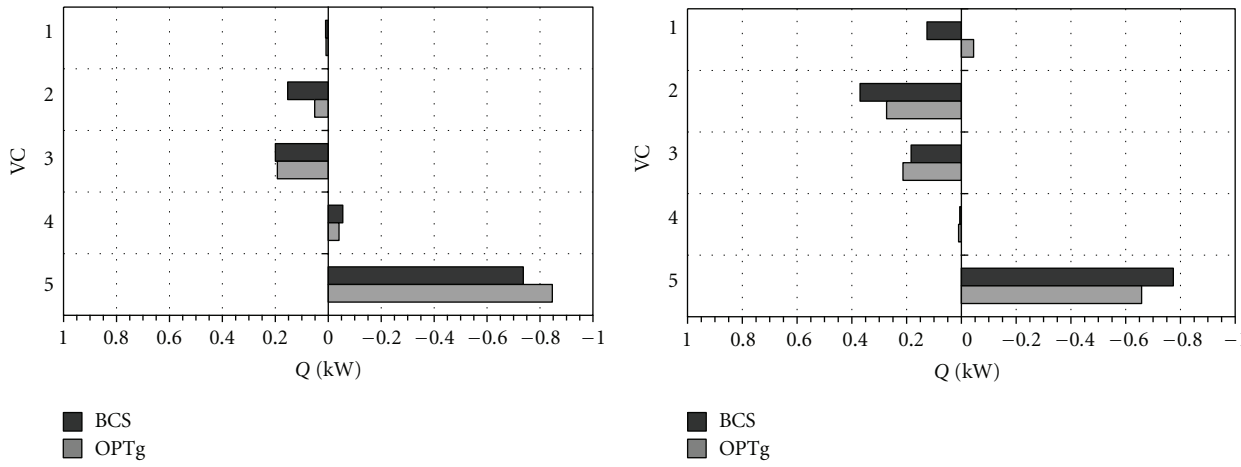

(a) West faces, w (inner border)

(b) East faces, e (outer border)

Figure 17: Enthalpic flow rate predictions across West (inner border) and East (outer border) of the air curtain control volumes, per unit length—OPTg case study.

i: Component of cartesian directions according to x, y, and z
inf: Infiltration, Inferior
lat: Latent component
m: Mixture
prod: Food products
sen: Sensible component.

Greek Symbols

α: Thermal entrainment factor (without PBP air flow)
ε: Porosity
ϕ: Relative humidity, (%)
γ: Grille angle, (°)
μ: Viscosity, ($\mathrm{kg\,m^{-1}\,s^{-1}}$)
ρ: Density, ($\mathrm{kg\,m^{-3}}$)
ω: Absolute humidity, ($\mathrm{kg_v/kg_a}$); Rotation speed, (rpm).

Acronyms

BC: Boundary Condition
BCS: CFD Base Case Study
DAG: Discharge Air Grille
OPTγ: CFD parametric study of the air discharge and return angles influence on the global performance
OPTd: CFD parametric study of the internal duct deflectors (guides and convergents) influence on the global performance
OPTg: CFD global optimization performance model
OPTp: CFD parametric study of the diameter and density perforation of the back panel influence on the global performance
PBP: Perforated Back Panel
OPTv: CFD parametric study of the fans velocity influence on the global performance
RAG: Return Air Grille
TEF: Thermal Entrainment Factor
VC: Volume of Control.

Acknowledgment

The authors wish to acknowledge the support of JORDÃO Cooling Systems, Guimarães, Portugal (http://www.jordao.com/).

References

[1] D. Westphalen, R. Zogg, A. Varon, and M. Foran, "Energy savings potential for commercial refrigeration equipment," in *Final Report Prepared for Building Equipment Division Office of Building Technologies*, A. D. Little, Ed., U.S. Department of Energy e DOE, Cambridge, Mass, USA, 1996.

[2] P. D. Gaspar, L. C. Carrilho Gonçalves, and R. A. Pitarma, "Experimental analysis of the thermal entrainment factor of air curtains in vertical open display cabinets for different ambient air conditions," *Applied Thermal Engineering*, vol. 31, no. 5, pp. 961–969, 2011.

[3] Freedonia, *World Commercial Refrigeration Equipment—Industry Study with Forecasts to 2014 & 2019*, The Freedonia Group, Cleveland, Ohio, USA, 2011.

[4] IPCC, Climate Change 2007. Intergovernmental Panel on Climate Change (IPCC) Secretariat, 2007.

[5] P. M. A. Miranda, F. E. S. Coelho, A. R. Tomé et al., "20th century portuguese climate and climate scenarios," in *Climate Change in Portugal: Scenarios, Impacts and Adaptation Measures*, F. D. Santos, K. Forbes, and R. Moita, Eds., Gradiva, 2002.

[6] N. J. Smale, J. Moureh, and G. Cortella, "A review of numerical models of airflow in refrigerated food applications," *International Journal of Refrigeration*, vol. 29, no. 6, pp. 911–930, 2006.

[7] T. Norton and D. W. Sun, "Computational fluid dynamics (CFD)—an effective and efficient design and analysis tool for the food industry: a review," *Trends in Food Science and Technology*, vol. 17, no. 11, pp. 600–620, 2006.

[8] G. Cortella, M. Manzan, and G. Comini, "CFD simulation of refrigerated display cabinets," *International Journal of Refrigeration*, vol. 24, no. 3, pp. 250–260, 2001.

[9] H. K. Navaz, R. Faramarzi, M. Gharib, D. Dabiri, and D. Modarress, "The application of advanced methods in analyzing the performance of the air curtain in a refrigerated display case," *Transactions of the ASME Journal of Fluids Engineering*, vol. 124, no. 3, pp. 756–764, 2002.

[10] M. Axell and P. Fahlén, "Design criteria for energy efficient vertical air curtains in display cabinets," in *Proceedings of the 21st IIR International Congress of Refrigeration*, IIR, Washington, DC, USA, 2003.

[11] H. K. Navaz, B. S. Henderson, R. Faramarzi, A. Pourmovahed, and F. Taugwalder, "Jet entrainment rate in air curtain of open refrigerated display cases," *International Journal of Refrigeration*, vol. 28, no. 2, pp. 267–275, 2005.

[12] A. M. Foster, M. Madge, and J. A. Evans, "The use of CFD to improve the performance of a chilled multi-deck retail display cabinet," *International Journal of Refrigeration*, vol. 28, no. 5, pp. 698–705, 2005.

[13] Y. G. Chen, "Parametric evaluation of refrigerated air curtains for thermal insulation," *International Journal of Thermal Sciences*, vol. 48, no. 10, pp. 1988–1996, 2009.

[14] Y. G. Chen and X. L. Yuan, "Experimental study of the performance of single-band air curtains for a multi-deck refrigerated display cabinet," *Journal of Food Engineering*, vol. 69, no. 3, pp. 261–267, 2005.

[15] I. Gray, P. Luscombe, L. McLean, C. S. P. Sarathy, P. Sheahen, and K. Srinivasan, "Improvement of air distribution in refrigerated vertical open front remote supermarket display cases," *International Journal of Refrigeration*, vol. 31, no. 5, pp. 902–910, 2008.

[16] P. D'Agaro, G. Cortella, and G. Croce, "Two- and three-dimensional CFD applied to vertical display cabinets simulation," *International Journal of Refrigeration*, vol. 29, no. 2, pp. 178–190, 2006.

[17] P. D. Gaspar, L. C. C. Gonçalves, and R. A. Pitarma, "Detailed CFD modelling of open refrigerated display cabinets," *Modelling and Simulation in Engineering*, vol. 2012, Article ID 973601, 17 pages, 2012.

[18] R. I. Issa, "Solution of the implicitly discretized fluid flow equations by operator-splitting," *Journal of Computational Physics*, vol. 62, pp. 40–65, 1985.

[19] B. van Leer, "Towards the ultimate conservative difference scheme. V. A second-order sequel to Godunov's method," *Journal of Computational Physics*, vol. 32, no. 1, pp. 101–136, 1979.

[20] EN-ISO Standard 23953, *Refrigerated Display Cabinets, Parts 1 and 2*, ISO—International Organization for Standardization, Geneva, Switzerland, 2005.

[21] P. D. Gaspar, L. C. C. Gonçalves, and R. A. Pitarma, "Experimental analysis of the thermal entrainment three dimensional effects in recirculated air curtains," in *Proceedings of the 10th International Conference on Air Distribution in Rooms (Roomvent '07)*, Helsinki, Finland, 2007.

[22] A. M. Foster, M. J. Swain, R. Barrett, P. D'Agaro, and S. J. James, "Effectiveness and optimum jet velocity for a plane jet air curtain used to restrict cold room infiltration," *International Journal of Refrigeration*, vol. 29, no. 5, pp. 692–699, 2006.

[23] J. J. Costa, L. A. Oliveira, and M. C. G. Silva, "Energy savings by aerodynamic sealing with a downward-blowing plane air curtain—a numerical approach," *Energy and Buildings*, vol. 38, no. 10, pp. 1182–1193, 2006.

[24] L. P. C. Neto, M. C. G. Silva, and J. J. Costa, "On the use of infrared thermography in studies with air curtain devices," *Energy and Buildings*, vol. 38, no. 10, pp. 1194–1199, 2006.

[25] F. C. Hayes and W. F. Stoecker, "Design data for air curtains," *ASHRAE Transactions*, vol. 75, no. 2, pp. 168–180, 1969.

[26] K. Z. Yu, G. L. Ding, and T. J. Chen, "A correlation model of thermal entrainment factor for air curtain in a vertical open display cabinet," *Applied Thermal Engineering*, vol. 29, no. 14-15, pp. 2904–2913, 2009.

[27] B. S. Field and E. Loth, "Entrainment of refrigerated air curtains down a wall," *Experimental Thermal and Fluid Science*, vol. 30, no. 3, pp. 175–184, 2006.